

# Constant Factor Time Optimal Multi-Robot Routing on High-Dimensional Grids in Mostly Sub-Quadratic Time

Jingjin Yu <sup>\*</sup>

December 3, 2024

## Abstract

Let  $G = (V, E)$  be an  $m_1 \times \dots \times m_k$  grid. Assuming that each  $v \in V$  is occupied by a robot and a robot may move to a neighboring vertex in a step via synchronized rotations along cycles of  $G$ , we first establish that the arbitrary reconfiguration of labeled robots on  $G$  can be performed in  $O(k \sum_i m_i)$  makespan and requires  $O(|V|^2)$  running time in the worst case and  $o(|V|^2)$  when  $G$  is non-degenerate (i.e., nearly one dimensional). The resulting algorithm, iSAG, provides average case  $O(1)$ -approximate (i.e., constant factor) time optimality guarantee. In the case when all dimensions are of similar size  $O(|V|^{\frac{1}{k}})$ , the running time of iSAG approaches a linear  $O(|V|)$ . Define  $d_g(p)$  as the largest distance between individual initial and goal configurations over all robots for a given problem instance  $p$ , building on iSAG, we develop the PARTITIONANDFLOW (PAF) algorithm that computes  $O(d_g(p))$  makespan solutions for  $k = 2, 3$  using mostly  $o(|V|^2)$  running time. PAF provides worst case  $O(1)$ -approximation regarding solution time optimality. We note that the worst case running time for the problem is  $\Omega(|V|^2)$ .

## 1 Introduction

In this work, we study the time optimal multi-robot routing or path planning problem on  $k$  dimensional grids and grid-like settings, with the assumption that each vertex of the grid is occupied by a labeled robot, i.e., the robot density is maximal. Our work brings several technical breakthroughs:

- On a  $k \geq 2$  (assuming  $k$  is a constant) dimensional grid  $G = (V, E)$ , our algorithm, iSAG, improves the running time of the *average case*  $O(1)$ -approximate (makespan) time optimal SPLITANDGROUP (SAG) algorithm from [1] from  $O(|V|^3)$  to a sub-quadratic  $o(|V|^2)$  for most cases and  $O(|V|^2)$  in the worst case (when  $G$  is degenerate and nearly one dimensional). The problem has a worst case time complexity lower bound of  $\Omega(|V|^2)$ .
- Define  $d_g(p)$  as the largest distance between individual initial and goal configurations over all robots for a given problem instance  $p$ , building on iSAG, we develop the PARTITIONANDFLOW (PAF) algorithm that computes  $O(d_g(p))$  makespan solutions for two and three dimensions in mostly  $o(|V|^2)$  time and  $O(|V|^2)$  time in the worst case. PAF provides *worst case*  $O(1)$ -approximate guarantee on time optimality. We note that PAF is developed independently of a key result from [2] that achieves the same effect for two dimensions only.
- Certain techniques in our work, which help enable the near optimal running time for iSAG and PAF, may be of independent interest, including:
  - We provide a shuffling procedure based on bipartite matching that allows the arbitrary redistribution of a group of unlabeled robots on arbitrary-dimensional grids (Theorem 5).
  - We provide an efficient procedure, also based on matching, that decouples an  $f > 0$  circulation into  $f$  unit circulations on arbitrary graphs (Theorem 13).

<sup>\*</sup>Jingjin Yu is with the Department of Computer Science, Rutgers University at New Brunswick. E-mails: jingjin.yu@cs.rutgers.edu.

From the practical standpoint, our results are of significance in multiple application domains including robotics and network routing. Particularly, in robotics, our results imply that even in highly dense settings, if among a group of labeled robots the maximum distance between a robot and its goal is of distance  $d_g$ , then it is possible to compute a routing plan that solves the entire problem that requires  $O(d_g)$  makespan in only quadratic time, assuming that the robots travel at no faster than unit speed. Further exploration of the algorithmic insights from our work may lead to more optimal coordination algorithms for applications including warehousing [3], automated container port management [4], and coordinated aerial flight [5]. As noted in [2], algorithms like PAF also help resolve open questions regarding routing strategies for interconnected mesh networks. Indeed, solving multi-robot routing on grid and grid-like structures is equivalent to finding vertex disjoint paths in the underlying network, extended over discrete time steps.

**Related work.** Multi-robot path planning, from both the algorithmic and the application perspectives, has been studied extensively [6–20], covering many application domains [5, 21–29]. Multi-robot path and motion planning is known to be computationally hard under continuous settings [30, 31], even when the robots are unlabeled [32, 33]. While the general multi-robot motion planning problem seems rather difficult to tackle, relaxed unlabeled continuous problems are solvable in polynomial time even near optimally [15, 34].

Restricting our attention to the discrete and labeled setting, in contrast to the continuous setting, feasible solutions are more readily computable. Seminal work by Kornhauser et al. [35], which builds on the work by Wilson [36], establishes that a discrete instance can be checked and solved in  $O(|V|^3)$  time on a graph  $G = (V, E)$ . Feasibility test can in fact be completed in linear time [37–39]. Optimal solutions remain difficult to compute in the discrete settings, however, even on planar graphs [2, 40]. Whereas many algorithms have been proposed toward optimally solving the discrete labeled multi-robot path planning problems [11, 41–48], few provide simultaneous guarantees on solution optimality and (polynomial) running time. This leads to the development of polynomial time methods that also provide these desirable guarantees [1, 2].

## 2 Preliminaries

Let  $G = (V, E)$  be a simple, undirected, and connected graph. A set of  $n \leq |V|$  robots labeled 1– $n$  may move synchronously on  $G$  in a collision-free manner described as follows. At integer (time) steps starting from  $t = 0$ , each robot must reside on a unique vertex  $v \in V$ , inducing a *configuration*  $X_t$  of the robots as an injective map  $X_t : \{1, \dots, n\} \rightarrow V$ , specifying which robot occupies which vertex at step  $t$  (see Fig. 1). From step  $t$  to step  $t + 1$ , a robot may *move* from its current vertex to an adjacent one under two collision avoidance constraints: (i)  $X_{t+1}$  is injective, i.e., each robot occupies a unique vertex, and (ii) for  $1 \leq i, j \leq n$ ,  $i \neq j$ ,  $X_t(i) = X_{t+1}(j) \rightarrow X_t(j) \neq X_{t+1}(i)$ , i.e., no two robots may *swap* locations in a single step. If all individual robot moves between some  $X_t$  and  $X_{t+1}$  are valid (i.e., collision-free), then  $M_t = (X_t, X_{t+1})$  is a valid *move* for all robots. Multiple such moves can be chained together to form a sequence of moves, e.g.,  $(X_t, X_{t+1}, \dots, X_{t+\Delta t})$ .

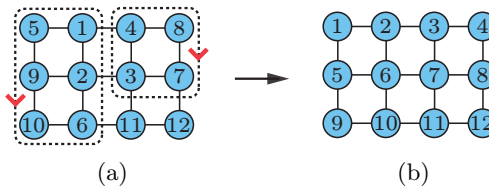


Figure 1: Graph-theoretic formulation of the multi-robot path planning problem. (a) A configuration of 12 robots on a  $4 \times 3$  grid. (b) A configuration that is reachable from (a) in a single synchronous move through simultaneous rotations of robots along two disjoint cycles.

Under this model, a multi-robot path planning problem (MPP) instance is fully specified with a 3-tuple  $(G, X_I, X_G)$  in which  $X_I = X_0$  and  $X_G$  are the initial and goal configurations, respectively. To handle the most difficult case, we assumed that  $n = |V|$ , i.e., the number of robots is the maximum possible under the model. We note that the case of  $n' < |V|$  may be reduced to the  $n = |V|$  case by arbitrarily placing  $(|V| - n')$  “virtual” robots on vertices that are empty as indicated by  $X_I$  and  $X_G$ . An algorithm for the  $n = |V|$  case is then also an algorithm for the  $n' < |V|$  case via the reduction.

For this study,  $G$  is assumed to be a  $k$ -dimensional ( $k \geq 2$ ) grid graph, i.e.,  $G$  is an  $m_1 \times \dots \times m_k$  grid with  $|V| = \prod_{i=1}^k m_i$ . Without loss of generality, throughout the paper we always assume that  $m_1 \geq \dots \geq m_k \geq 2$  and  $|V| \geq 6$  (note that constant sized problems can be solved in  $O(1)$  makespan through first doing brute force search and then direct solution look up, which takes constant time). Such a grid graph  $G$  is also meant whenever the term *grid* is used in the paper without further specifications. We say  $G$  is *degenerate* if  $m_1 = \Omega(|V|)$ , which implies that all other dimensions are of constant sizes, i.e.,  $G$  is mostly one-dimensional. Otherwise,  $G$  is *non-degenerate*. Since the most interesting cases are  $k = 2, 3$  due to their relevance in applications, these cases are treated with additional attention.

Given an MPP instance and a feasible solution, as a sequence of moves  $M = (X_I = X_0, X_1, \dots, X_{t_f} = X_G)$  that takes  $X_I$  to  $X_G$ , we define the solution's *makespan* as the length  $t_f$  of the sequence. For an MPP instance  $p = (G, X_I, X_G)$ , let  $d(v_1, v_2)$  denote the distance between two vertices  $v_1, v_2 \in V$ , assuming each edge has unit length. We define the *distance gap* between  $X_I$  and  $X_G$  as

$$d_g(p) = \max_{1 \leq i \leq |V|} d(X_I(i), X_G(i)),$$

which is an underestimate of the minimum makespan for  $p$ . The main aim of this work is to establish a polynomial time algorithm that computes solutions with  $O(d_g(p))$  makespan for an arbitrary instance  $p$  whose underlying grid are of dimensions  $k = 2, 3$ . In other words, the algorithm produces, in the worst case,  $O(1)$ -approximate makespan optimal solutions. Note that, on an  $m_1 \times \dots \times m_k$  grid,  $d_g(p) \leq \sum_{i=1}^k (m_i - 1)$ .

### 3 Improved Average Case $O(1)$ -Approximate Makespan Algorithm

Our worst case  $O(1)$ -approximate algorithm makes use of, as a subroutine, an average case  $O(1)$ -approximate algorithm for the same problem that improves over the SPLITANDGROUP (SAG) algorithm from [1]. Main properties of SAG are summarized in the following theorem.

**Theorem 1** ([1]). *Let  $(G, X_I, X_G)$  be an MPP instance with  $G = (V, E)$  being an  $m_1 \times m_2$  grid. Then, a solution with  $O(m_1 + m_2)$  makespan can be computed in  $|V|^3$  time.*

To be able to state our improvements over SAG, we briefly describe how SAG operates on an  $m_1 \times m_2$  grid  $G$ . SAG recursively splits  $G$  into halves along a longer dimension. During the first iteration,  $G$  is *split* into two  $\frac{m_1}{2} \times m_2$  grids (assuming without loss of generality that  $m_1$  is even),  $G_1$  and  $G_2$ . Then, all robots whose goals belong to  $G_2$  will be routed to  $G_2$ . This will also force all robots whose goals belong to  $G_1$  to be moved to  $G_1$  because  $G$  is fully occupied. This effectively partitions all robots on  $G$  into two equivalence classes (those should be in  $G_1$  and those should be in  $G_2$ ); there is no need to distinguish the robots within each class during the current iteration. This is the *grouping* operation in SAG. Fig. 2 illustrates graphically what is to be achieved in the grouping operation in an iteration of SAG.

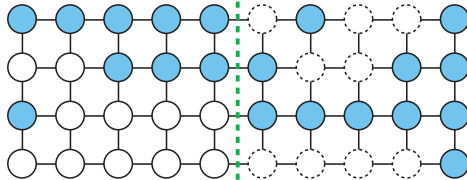


Figure 2: On a  $10 \times 4$  grid, the shaded robots have goals on the right  $5 \times 4$  grid. The grouping operation of an SAG iteration seeks to move the 9 shaded robots on the left  $5 \times 4$  grid to exchange with the 9 unshaded robots marked with dashed boundaries on the right  $5 \times 4$  grid.

To be able to move the robots to the desired halves of  $G$ , it was noted [48] that an exchange of two robots can be realized on a  $3 \times 2$  grid using a constant number of moves (Fig. 3).

The local “swapping” primitives can be executed in parallel on  $G$ , which implies Lemma 2 as follows. An illustration of the operation is provided in Fig. 4.

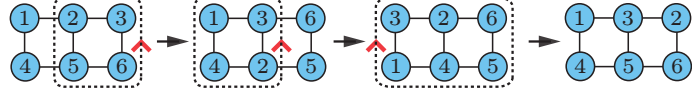


Figure 3: Robots 2 and 3 may be “swapped” using three synchronous moves on a  $3 \times 2$  grid. This implies that arbitrary configuration on a  $3 \times 2$  grid can be realized in a constant number of moves.

**Lemma 2** (Lemma 6 in [1]). *On a length  $\ell$  path embedded in a grid, a group of indistinguishable robots may be arbitrarily rearranged using  $O(\ell)$  makespan. Multiple such rearrangements on vertex disjoint paths can be carried out in parallel.*

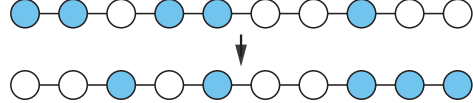


Figure 4: Assuming a length  $\ell$  path is embedded in a grid, Lemma 2 guarantees that the arbitrary distribution of a group of robots can be performed using  $O(\ell)$  make span.

Lemma 2 further implies Lemma 3. Fig. 5 illustrates graphically the operation realized by Lemma 3.

**Lemma 3** (Lemma 7 in [1]). *On a length  $\ell$  path embedded in a grid, two groups of robots, equal in number and initially located on two disjoint portions of the path, may exchange locations in  $O(\ell)$  makespan. Multiple such exchanges on vertex disjoint paths can be carried out in parallel.*

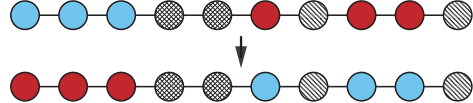


Figure 5: Assuming the grid-embedded path has a length of  $\ell$ , Lemma 3 guarantees that the swapping of the two separated groups of robots, up to  $\frac{\ell}{2}$  per group, can be done in  $O(\ell)$  make span without any net movement of other robots on the line.

Lemma 2 and Lemma 3 both demand a running time of  $O(\ell^2)$ . We note that some problems require  $\Omega(\ell^2)$  time to simply write down the solution, e.g., when  $\frac{\ell}{2}$  robots need to be moved on a path of length  $\ell$ . Several additional results were developed over Lemma 3 in [1] to complete the grouping operation, which involves complicated routing of robots on trees, embedded in a grid, that may overlap. We provide an alternative method that not only simplifies the process with better running time but also allows easy generalization to high dimensions. We note that, to complete the grouping operations, using the example from Fig. 2 for illustration, we only need to reconfigure robots on the left  $5 \times 4$  grid so that for each row, robots to be exchanged across the split line are equal in number (see Fig. 6). Lemma 3 then takes care of the rest.

To perform the reconfiguration, we begin by assigning labels to the robots as illustrated in Fig. 7 (see the description in the figure on how the labels are assigned in a straightforward manner, which takes linear time with respect to the size of the grid). These labels are only for pairing up robots for the reconfiguration; keep in mind that the shaded robots are in fact indistinguishable in the execution of the grouping operation.

With the labeling, we set up a bipartite graph as follows. One of the partite set  $\{v_i^1\}$  (e.g.,  $\{v_1^1, \dots, v_5^1\}$  in Fig. 8) represents the initial columns and the other set  $\{v_j^2\}$  (e.g.,  $\{v_1^2, \dots, v_5^2\}$  in Fig. 8) the goal columns. We draw an edge between  $v_i^1$  and  $v_j^2$  if a shaded robot labeled  $i$  ends up at a goal column  $j$ . For example, in Fig. 7, shaded robots with label 1 in (a) ends up at columns 1 and 2 in (b), yielding the edges  $(v_1^1, v_1^2)$  and  $(v_1^1, v_2^2)$  in Fig. 8. If a goal column  $j$  contains multiple shaded robots with label  $i$ , then multiple edges between  $v_i^1$  and  $v_j^2$  are added. Note that, if we also add the edges for the unshaded robots in Fig. 7 in

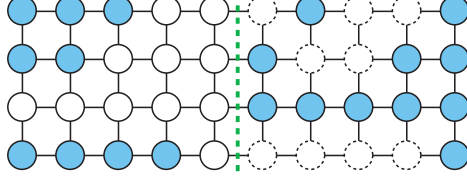


Figure 6: We would like to reconfigure robots on the left  $5 \times 4$  half of Fig. 2 to the configuration as shown. The right  $5 \times 4$  portion will not be touched in the operation. In this configuration, robots do not need to move between different rows to complete the grouping operation, using Lemma 3.

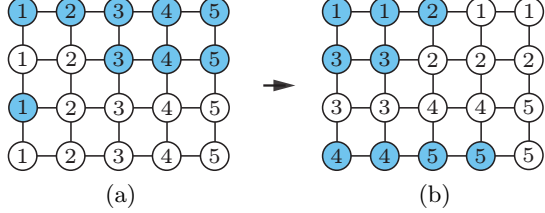


Figure 7: (a) and (b) correspond to the left  $5 \times 4$  grids from Fig. 2 and Fig. 6, respectively. We would like to reconfigure the shaded robots to go from (a) to (b) (ignoring the labels). In (a), shaded robots are assigned labels based on the column they belong to. In (b), from top to bottom and left to right, we sequentially assign each shaded labeled robot from (a) a goal. The same is done to the unshaded robots.

a similar manner, the bipartite graph will be  $d$ -regular where  $d$  is the number of rows in the original grid ( $d = 4$  in the provided example).

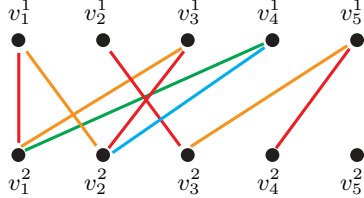


Figure 8: A bipartite graph constructed for rearranging robots. The 4 colorings of the edges indicate a possible set of 4 matchings, which are  $\{1 - 1, 2 - 3, 3 - 2, 5 - 4\}$  (red),  $\{1 - 2, 3 - 1, 5 - 3\}$  (orange),  $\{4 - 1\}$  (green),  $\{4 - 2\}$  (cyan).

With the bipartite graph constructed, we proceed to obtain a set of up to  $d$  maximum matchings. We note that this is always possible because our bipartite graph is a sub graph of a  $d$ -regular bipartite graph (By Hall's theorem [49], a perfect matching may be obtained on a  $d$ -regular bipartite graph, the removal of which leaves a  $(d - 1)$ -regular bipartite graph). From the obtained set of matchings (e.g., using Hopcroft-Karp [50]), we permute with Lemma 2 to distribute the robots vertically so that a robot matched in the  $i$ -th matching gets moved to the  $i$ -th row. In our example, the first set is  $\{1 - 1, 2 - 3, 3 - 2, 5 - 4\}$ , which means that a set of three shaded robots labeled 1, 2, 3, and 5 should be moved to the first row. Doing this for all matching sets shown in Fig. 7(a) yields the configuration in Fig. 9(a). Then, in a second round, the robots are permuted within their row, again using the matching result. In the example, the first matching set  $\{1 - 1, 2 - 3, 3 - 2, 5 - 4\}$  says that robots 1, 2, 3, and 5 on the first row should be moved to columns 1, 3, 2, and 4. We note that going from 1, 2, 3, 5 to 1, 3, 2, 4 is possible with Lemma 2 because the labels are nominal; we only need to move the four indistinguishable robots to columns 1, 2, 3, and 4. For the configuration in Fig. 9(a), this round yields the configuration in Fig. 9(b). We note that the bipartite matching technique mentioned here was due to [51], in which a variation of it is used for a different reconfiguration problem.

We observe that the labeled robots that need to be moved now are all in the correct columns. One last column permutation then moves the robots in place. In the example, this is going from Fig. 9(b) to Fig. 7(b).

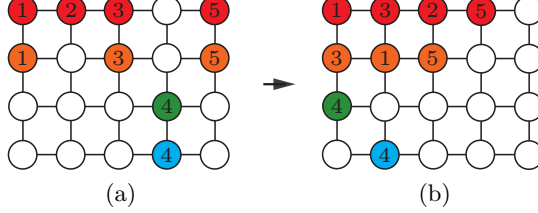


Figure 9: (a) The initial permutation of columns of Fig. 7(a) using the bipartite matching result. (b) A second row-based permutation of (a) using the bipartite matching result. Our procedure operates following the sequence Fig. 7(a)  $\rightarrow$  Fig. 9(a)  $\rightarrow$  Fig. 9(b)  $\rightarrow$  Fig. 7(b).

We summarize the the discussion in the following lemma.

**Lemma 4.** *On an  $m_1 \times m_2$  grid, the reconfiguration of a group of indistinguishable robots between two arbitrary configurations can be completed using  $O(m_1 + m_2)$  makespan in  $O(m_1^2 m_2 + m_1 m_2^2)$  time.*

*Proof.* The procedure is already fully described; here, we analyze its performance. The procedure operates in three phases, each requiring a makespan of either  $O(m_1)$  or  $O(m_2)$  (because only one dimension of the  $m_1 \times m_2$  grid is involved in each phase). The overall makespan is then  $O(m_1 + m_2)$ . Regarding the computation time, each invocation of the procedure from Lemma 2 or Lemma 3 on an  $m_1 \times m_2$  grid takes  $O(m_1^2)$  or  $O(m_2^2)$  time; doing these in parallel on the grid then takes  $O(m_1^2 m_2 + m_1 m_2^2) = O(m_1^2 m_2)$  time. For doing the bipartite matching, we may invoke an  $O(|E|)$  time matching algoithm [52]  $d$  times to get a  $O(d|E|)$  running time where  $d = m_2$  and  $|E_B| = m_1 m_2$  are the degree and the number of edges of the  $d$ -regular bipartite graph. The total time spent on matching is  $O(m_1 m_2^2)$ . The overall running time is then  $O(m_1^2 m_2 + m_1 m_2^2)$ .  $\square$

We now generalize Lemma 4 to  $k \geq 2$  dimensions.

**Theorem 5.** *On an  $m_1 \times \dots \times m_k$  grid, the reconfiguration of a group of indistinguishable robots between two arbitrary configurations can be completed using*

$$O\left(\sum_{i=1}^k m_i\right)$$

*makespan and requires time*

$$O\left(\left(\prod_{i=1}^k m_i\right)\left(\sum_{i=1}^k m_i\right)\right). \quad (1)$$

*Proof.* Since the case of  $k = 3$  is of practical importance, we first provide the proof for this case, which also outlines the inductive proof approach for general  $k$ . On an  $m_1 \times m_2 \times m_3$  grid, we partition the gird into  $m_1 m_2$  columns of size  $m_3$ , in the natural way. To build the bipartite graph, robots to be moved will be labeled based on the column it belongs to, yielding  $m_1 m_2$  labels. The goals for these robots are assigned sequentially, similar to how it is done in the 2D case. After building the bipartite graph as before and performing the matching, the robots to be moved are partitioned into  $m_3$  layers (a layer in the 3D case corresponds to a *row* in the 2D case) with each layer being an  $m_1 \times m_2$  grid.

Then, as in the 2D case, a column permutation is done for each of the  $m_1 m_2$  columns, in parallel. To be able to move the robots on each layer which is a  $m_1 \times m_2$  grid, we invoke Lemma 4 in parallel on all  $m_3$  layers. This is then followed by a final parallel column permutation.

To count the makespan, the initial and final column permutations require  $O(m_3)$  makespan and working with the layers requires  $O(m_1 + m_2)$  makespan, yielding a total makespan of  $O(m_1 + m_2 + m_3)$ . For running time, at the top layer, the bipartite matching process creates a bipartite graph  $G_B = (V_B, E_B)$  with  $|E_B| = m_1 m_2 m_3$ . The time for doing  $d = m_3$  matchings is then  $O(m_1 m_2 m_3^2)$ . The initial and final column permutation takes time  $O(m_1 m_2 m_3^2)$  (because we need to arrange  $m_1 m_2$  columns of size  $m_3$  each). For

handling the  $m_3$  layers of  $m_1 \times m_2$  grids, by Lemma 4, it takes time  $O(m_1^2 m_2 m_3 + m_1 m_2^2 m_3)$ . The overall running time is then  $O(m_1^2 m_2 m_3 + m_1 m_2^2 m_3 + m_1 m_2 m_3^2)$ .

For constructing the inductive proof, suppose for dimension  $k$ , our makespan hypothesis for reconfiguration is  $O(m_1 + \dots + m_k)$ . The running time hypothesis is as given in the theorem statement. For dimension  $k+1$ , the problem is first approached at the top level to generate  $m_{k+1}$  “layers” of size  $\prod_{i=1}^k m_i$  each (corresponding to a  $m_1 \times \dots \times m_k$  grid). After permuting  $\prod_{i=1}^k m_i$  columns of size  $m_{k+1}$ ,  $m_{k+1}$   $k$ -dimensional problems are then solved via the induction hypothesis. Lastly, another column permutation is performed to complete the reconfiguration.

To count the makespan required, we note that at dimension  $k$ , the initial and final column permutations require a makespan of  $O(m_{k+1})$  as all  $\prod_{i=1}^k m_i$  columns of size  $m_{k+1}$  can be operated on in parallel. By the induction hypothesis, the total makespan is then  $O(m_1 + \dots + m_{k+1})$ , which actually does not directly depend on the dimension. The running time for the first matching operation takes  $O((\prod_{i=1}^k m_i)m_{k+1}^2)$  time. The running time for the initial and final column permutations require calling the  $O(m_{k+1}^2)$  routine (Lemma 2)  $\prod_{i=1}^k m_i$  times, taking the same amount of time. By the induction hypothesis, handling the  $m_{k+1}$  layers take time  $m_{k+1}$  multiple of (1). Putting these together yields again (1) with  $k$  replaced by  $k+1$ .  $\square$

A case of special interest is when all  $m_i$ ,  $1 \leq i \leq k$ , are about the same.

**Corollary 6.** *On a  $k$ -dimensional grid with all sides having lengths  $O(|V|^{\frac{1}{k}})$ , the reconfiguration of a group of indistinguishable robots between two arbitrary configurations can be completed using  $O(k|V|^{\frac{1}{k}})$  makespan and  $O(|V|^{\frac{k+1}{k}})$  time.*

Replacing the tree-routing based grouping operation in SAG with the updated, staged grouping routine, we obtain the following improved result.

**Theorem 7.** *Let  $(G, X_I, X_G)$  be an MPP instance with  $G$  being an  $m_1 \times \dots \times m_k$  grid for some  $k \geq 2$ . Then, a solution with*

$$O(k \sum_{i=1}^k m_i)$$

*makespan can be computed in time*

$$O(k(\prod_{i=1}^k m_i)(\sum_{i=1}^k m_i)). \quad (2)$$

*Proof.* Similar to SAG, standard divide-and-conquer is applied that iteratively divides  $G$  and subsequent partitions into equal halves; the grouping operation is then applied. For the grouping operation, after reconfiguration on a half grid, a parallel invocation of Lemma 3 is needed to move the robots across the splitting boundary, which takes at most  $O(m_1^2 m_2 \dots m_k)$  time. Because  $O(m_1^2 m_2 \dots m_k)$  is already a term in (1), this additional operation does not contribute to more computation time in an iteration of SAG.

For a  $k$ -dimensional grid, in the first  $k$  iterations, we may choose the  $d$ -th round to divide dimension  $d$  into two halves (i.e.,  $m'_d = \frac{m_d}{2}$ ). Following this scheme, for the  $d$ -th round, the makespan is

$$O\left(\frac{m_1}{2} + \dots + \frac{m_{d-1}}{2} + m_d + \dots + m_k\right).$$

For computation time, we need to operate on  $2^{d-1}$  subproblems with each subproblem requiring time no more than

$$O(2^{-d+1}(\prod_{i=1}^k m_i)(\sum_{i=1}^k m_i)).$$

That is, each of the first  $k$  iterations takes no more time than (1). Tallying up, the first  $k$  rounds require makespan and running time as given in the theorem statement.

After  $k$  rounds of division, all dimensions are halved. To complete the next  $k$  rounds, the required makespan is halved and the computation time shrinks even more (since it's quadratic in at least one of the dimensions and super linear in the rest). Subsequently, the makespan and the running time for the first  $k$  rounds dominate.  $\square$

To distinguish our modification with SAG, we denote the improved SAG algorithm as iSAG. We mention that iSAG runs in quadratic  $O(|V|^2)$  time if we allow  $G$  to be degenerate, i.e.,  $m_1 = \Omega(|V|)$ . To see that this is true, we observe that the term inside (2) is bounded by

$$k^2 m_1 \prod_{i=1}^k m_i = k^2 |V|^2 \prod_{i=1}^{k-1} m_i^{-1} < k^2 2^{-k+1} |V|^2$$

because  $m_i \geq 2$ . The last term is  $O(|V|^2)$  since  $k^2 2^{-k+1}$  is bounded by some small constant. As noted, the quadratic bound is sometimes necessary when  $G$  is degenerate (see discussion following Lemma 3). We note that in this case, the running time lower bound can also be  $\Omega(|V|^2)$ . When  $G$  is non-degenerate, iSAG runs in a sub-quadratic  $o(|V|^2)$  time that approaches  $O(|V|)$ .

We conclude this section with a corollary, which will be useful later, that directly follows Corollary 6 and Theorem 7.

**Corollary 8.** *When all dimensions of the underlying grid are of similar magnitude, the makespan and computation time for solving an MPP instance are  $O(\sqrt{|V|})$  and  $O(|V|^{\frac{3}{2}})$ , respectively, for two dimensions. For three dimensions, these are  $O(|V|^{\frac{1}{3}})$  and  $O(|V|^{\frac{4}{3}})$ , respectively. For general  $k$ , these are  $O(k^2|V|^{\frac{1}{k}})$  and  $O(k^2|V|^{\frac{k+1}{k}})$ , respectively.*

## 4 From Average Case to Worst Case: A Solution Sketch for Two Dimensions

In this section, we highlight, at a high level, why solution produced by iSAG can be rather undesirable in practice and how its shortcomings can be addressed with the PARTITIONANDFLOW (PAF) algorithm. In sketching PAF, we resort to the frequent use of figures to illustrate the important steps. We emphasize that the steps explained using these pictorial examples are also rigorously proved to be correct later in Section 5. Full optimality and running time analysis will also be delayed until then.

### 4.1 The Difficulty

Given an MPP instance  $p = (G, X_I, X_G)$ , let the makespan computed by iSAG be denoted as  $d_{iSAG}(p)$ . From an algorithmic perspective, iSAG delivers  $O(1)$ -approximate makespan optimal solutions *on average*, i.e., for a fixed  $G$ , let all instances of MPP on  $G$  be  $\{p_i = (G, X_I^i, X_G^i)\}$ , then iSAG ensures the quantity (as a sum of ratios)

$$\sum_i \frac{d_{iSAG}(p_i)}{d_g(p_i)}$$

is a constant. A key assumption in the average case analysis is that all instances  $\{p_i\}$  for a fixed  $G$  are equally likely, implying a uniform distribution of problem instances. When this assumption does not hold, as is the case in many practical scenarios, iSAG no longer guarantees  $O(1)$  approximation. Such cases may be illustrated with a simple example. On an  $m \times m$  grid, let an MPP instance be constructed so that to reach the goal configuration, all robots on the outer boundary must rotate synchronously once in the clockwise direction (see Fig. 10). The minimum makespan of the instance is 1 but iSAG will incur a makespan of  $O(m)$  due to its divide-and-conquer approach that agnostically divide the grid in the middle.

On the other hand, if a polynomial time algorithm can be constructed that always produces  $O(d_g(p))$  makespan for an arbitrary MPP instance  $p$ , then  $O(1)$ -approximate optimal solution can always be guaranteed. Naturally, such an algorithm will necessarily require some form of divide-and-conquer on top of which the *flow* of robots at the *global* scale must also be dealt with. The key to establishing such an algorithm is to be able to recognize the global flow to generate appropriate *local* routing plans. In terms of the example illustrated in Fig. 10, the two darker shaded (red) robots must be routed *locally* across the thick dashed (green) boundary lines. This implies that all the shaded robots must more or less move along synchronously around the cycle. A main challenge is how to realize such local-global coordination when many such cyclic flows are entangled under maximum robot density.

Here, we mention that the special case of  $d_g(p) = 1$  can be easily handled for an arbitrary dimension  $k$ .

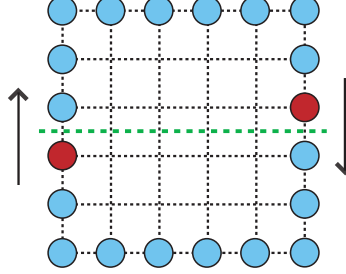


Figure 10: An MPP instance on an  $m \times m$  grid. Solving the instance requires all robots on the outside perimeter to move clockwise once. iSAG will first cause the two (red, darker shaded) robots to exchange locations, which induces a makespan of  $O(m)$ .

**Proposition 9.** Let  $G$  be  $k$  dimensional grid with  $k \geq 2$  and let  $p = (G, X_I, X_G)$  be an MPP instance with  $d_g(p) = 1$ . Then an  $O(1)$  makespan plan for solving  $p$  can be computed in  $O(k|V|)$  time.

*Proof.* In this case, for a given robot  $i$ , if  $X_I(i) \neq X_G(i)$ , its goal is just one edge away. Starting from any robot  $i$ , the vertices  $v_1 = X_I(i), v_2 = X_G(i), v_3 = X_G(X_I^{-1}(v_2)), v_4 = X_G(X_I^{-1}(v_3)), \dots$  induce a cycle on  $G$ . When such a cycle has two vertices, this represents an exchange of two robots. Using parallel swapping operations, such exchanges can be completed in  $O(1)$  makespan, which leave only simple cycles on  $G$  that are all disjoint. Robots on these simple cycles can then move to their goals in a single synchronous move. The total makespan is then  $O(1)$  and to compute the plan is to simply write down the cycles, which takes time linear with respect to the size of the grid. The factor  $k$  comes from the search branching factor.  $\square$

## 4.2 Sketch of PartitionAndFlow

In sketching the PAF algorithm, we remark that PAF essentially works on a problem  $(G, X_I, X_G)$  by gradually updating  $X_I$ . That is, it first creates some intermediate  $X_G^1$  based on  $X_I$  and  $X_G$  and solve the problem  $(G, X_I, X_G^1)$ , leaving a new problem  $(G, X_G^1, X_G)$ . Then, it repeats the process to create and solve another problem  $(G, X_G^1, X_G^2)$ , resulting a new problem  $(G, X_G^2, X_G)$ . The process continues until  $X_I$  is updated to eventually match  $X_G$ . It is important to keep this in mind in reading the sketch of PAF.

In our description of PAF in this section, a two-dimensional,  $m_1 \times m_2$  grid will be assumed. The generalization to a  $k$ -dimensional grid will use the same general approach but require more involved treatment. As the name suggests, PAF partitions an MPP instance on a grid into small pieces and organize the flow of robots through these pieces globally. The partition is essentially a form of decoupling that includes and is more general than iSAG's half-half splitting scheme.

For a given MPP instance  $p = (G, X_I, X_G)$  with  $G$  being an  $m_1 \times m_2$  grid, PAF starts by computing  $d_g(p)$ , the distance gap for the problem<sup>1</sup>. In the main case,  $d_g = o(m_2)$ . That is, for any robot  $i$ ,  $d(X_I(i), X_G(i)) = o(m_2)$ . This means that  $G$  may be partitioned into square cells of sizes  $5d_g \times 5d_g$  each. This is the *partition* operation in PAF (see Fig. 11 for an illustration). For the moment, we assume that a perfect partition can be achieved, i.e.,  $m_1$  and  $m_2$  are both integer multiples of  $5d_g$ ; the assumption is justified in Section 5.

The partition scheme, as a refinement to the splitting scheme from iSAG, has the property that only robots of distance  $d_g$  from a cell boundary may have goals outside the cell by the definition of  $d_g$  (for more details, see Fig. 12). This means that between two cells that share a vertical or horizontal boundary, at most  $10d_g^2$  robots need to cross that boundary. If we only count the net exchange, then the number reduces to  $5d_g^2$ .

Over the partition, PAF will build a flow between the cells treating each cell as a node in a graph. To be able to translate the flow into feasible robot movements, the flow should only happen between adjacent cells that share a boundary. However, as illustrated in Fig. 12, it is possible for a robot to have initial and goal configurations that are separated into *diagonally adjacent* cells which do not share boundaries. To resolve

<sup>1</sup>Henceforth, we use  $d_g$  in place of  $d_g(p)$  because the instance is always fixed (but arbitrary);  $d_g(p)$  is otherwise only used in theorem statements when a problem  $p$  is being specified.

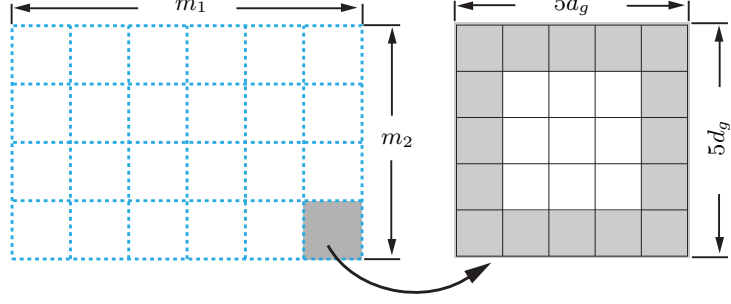


Figure 11: Partitioning of an  $m_1 \times m_2$  grid into  $6 \times 4$  cells. Each cell has a size of  $5d_g \times 5d_g$ . Within a cell (the figure on the right), only robots located of a distance no more than  $d_g$  from the border may have goals outside the cell.

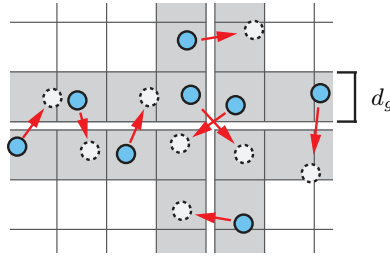


Figure 12: An illustration of the  $d_g$  thick boundary areas of four adjacent cells. Any net robot exchange between two cells must happen in this region by the definition of  $d_g$ .

this, we may update the goals for these robots using robots from another cell that is adjacent to both of the involved cells. Fig. 13 illustrates how one such robot can be processed. We call this operation *diagonal rerouting*, which will create a new configuration  $X_G^1$  of the robots on  $G$ . iSAG is then invoked to solve  $(G, X_I, X_G^1)$ . iSAG will do so locally on  $4d_g \times 4d_g$  regions that span equal parts of four adjacent cells.

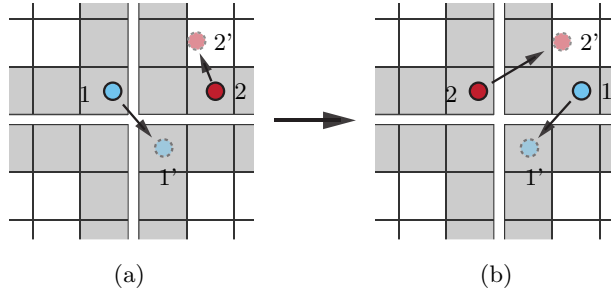


Figure 13: (a) At the boundary between four cells, robot 1 has initial and goal configurations (vertices) spanning two diagonally adjacent cells. In the top right cell which is adjacent to both the top left and bottom right cells, there exists a robot that has its goal vertex in the same cell. (b) By swapping the robots 1 and 2 using iSAG, no robot needs to cross cell boundaries diagonally.

Then, PAF creates another intermediate configuration  $X_G^2$  for moving robots between each vertical or horizontal cell boundary so that between any two cells, robots will only need to move in a single direction when crossing a cell boundary. That is, for each cell boundary, iSAG is called to “cancel out” non-net robot movements, as illustrated in Fig. 14, leaving only uni-directional robot movements across cells. We call this operation *flow cancellation*.

The net robot movement across cell boundary induces a flow over the cells (see Fig. 15(a)). Because each cell contains a fixed number of robots, the incoming and outgoing flow at each cell (node) must be

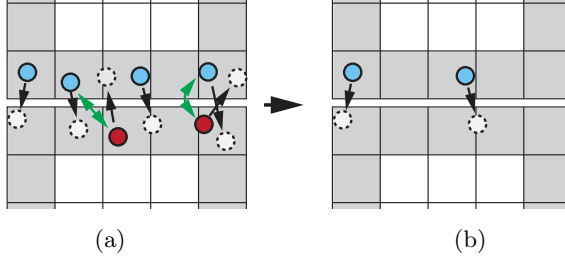


Figure 14: (a) There are four robots in the top cell and two robots in the bottom cell that need to move across the horizontal boundary. (b) Through an arbitrary matching (indicated with double sided arrows) of two pairs of robots' initial configurations and applying iSAG to swap them, the robot movements across the boundary are now unidirectional.

equal. This means that all such flows must form a valid *circulation*<sup>2</sup> over the graph formed by cells as nodes. The flow between two adjacent cells is no more than  $6d_g^2$  (to be established later). The circulation can then be decomposed into  $6d_g^2$  *unit circulations* (Fig. 15(b)). These unit circulations can be translated into coordinated *global* robot movements that require any robot to travel only *locally* at most a distance of  $O(d_g)$ . The translation amounts to creating another configuration  $X_G^3$ .  $(G, X_G^2, X_G^3)$  is also solved using iSAG.

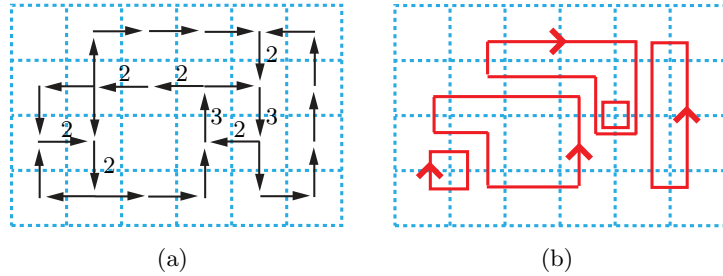


Figure 15: (a) Induced circulation (network) from required robot movements. The numbers denote the total flow on a given edge. The edges without numbers have unit flows. (b) After decomposition, the circulation can be turned into unit circulations on simple cycles.

After the preparation phase is done, the scheduled global robot movements can be directly executed, yielding a new configuration  $X_G^4$ . The configuration  $X_G^4$  has the property that every robot is now in the  $5d_g \times 5d_g$  partitioned cell where its goal resides. iSAG can then be invoked to solve  $(G, X_G^4, X_G)$  (iSAG is invoked at the cell level). Throughout the process, each robot only needs to move a distance of  $O(d_g)$  and calls to iSAG can be performed in parallel, yielding an overall makespan of  $O(d_g)$ . Before presenting the details of PAF in Section 5, we outline the steps of PAF in Algorithm 1. We emphasize that the outline is provided at a very high level that summarizes the sketch of PAF and only covers the main case in 2D.

In closing this section, we note that in providing the details of PAF in Section 5, objects of minor importance, including the temporary configurations (e.g.,  $X_G^i$ 's) and actual robot movement plans (e.g.,  $M^i$ 's), will be omitted in the description. However, sufficient details are provided if a reader is interested in deriving these objects.

## 5 PartitionAndFlow in 2D: the Details

At this point, we make the assumption that for the rest of the paper (unless stated explicitly otherwise), for a given problem with  $G$  being an  $m_1 \times \dots \times m_k$  grid,  $d_g = o(m_1)$ . Otherwise,  $d_g(p) = \Omega(m_1)$  and we may simply invoke iSAG to solve the problem. We note that this is a different condition than requiring  $G$  being non-degenerate.

<sup>2</sup>A circulation is essentially a valid flow over a network without source and sink nodes. That is, the incoming flows and outgoing flows at every node of the network are equal in magnitude.

---

**Algorithm 1:** PAFMAINCASE2D( $G, X_I, X_G$ )

---

**Input :**  $G = (V, E)$ : an  $m_1 \times m_2$  grid graph  
 $X_I$ : initial configuration  
 $X_G$ : goal configuration

**Output:**  $M = \langle M_1, M_2, \dots \rangle$ : a sequence of moves

%Partition  $G$ ;  $G_S$  represents the partition

- 1  $G_S \leftarrow \text{PARTITION}(G, X_I, X_G)$
- 2 %Orienting flows on  $G_S$
- 3  $M^1, X_G^1 \leftarrow \text{DIAGOALREROUTE}(G, G_S, X_I, X_G)$
- 4  $M^2, X_G^2 \leftarrow \text{FLOWCANCELLATION}(G, G_S, X_G^1, X_G)$
- 5 %Flow decomposition and global route preparation;  $P$  are the routes
- 6  $M^3, X_G^3, P \leftarrow \text{DECOMPOSEFLOW}(G, G_S, X_G^2, X_G)$
- 7 %Global robot routing
- 8  $M^4, X_G^4 \leftarrow \text{GLOBALROUTING}(G, P)$
- 9 %Final local robot routing
- 10  $M^5 \leftarrow \text{FINALLOCALROUTE}(G, G_S, X_G^4, X_G)$
- 11 **return**  $M^1 + M^2 + M^3 + M^4 + M^5$

---

We now proceed to provide the full description of how to piece together PAF. The goal of this section is to establish the following main result on the existence of a polynomial time algorithm (PAF) for computing worst case  $O(1)$ -approximate makespan optimal solution for MPP, in two dimensions.

**Theorem 10.** *Let  $p = (G, X_I, X_G)$  be an arbitrary MPP instance with  $G$  being an  $m_1 \times m_2$  grid. A solution for  $p$  with  $O(d_g(p))$  makespan can be computed in  $O(m_1 m_2 d_g^2)$  deterministic time or  $O(m_1 m_2 d_g + m_1 m_2 \log \frac{m_1 m_2}{d_g^2})$  expected time.*

Beside the main case outlined in Section 4, there is also a special case that needs to be analyzed in proving Theorem 10, depending on the magnitude of  $d_g$  relative to  $m_1$  and  $m_2$ . The cases for  $d_g = o(m_1)$  are divided into two disjoint cases: (i)  $d_g = \Omega(m_2)$  and (ii)  $d_g = o(m_2)$ . The first case can be readily addressed.

**Lemma 11.** *Let  $p = (G, X_I, X_G)$  be an arbitrary MPP instance in which  $G$  is an  $m_1 \times m_2$  grid with  $d_g(p) = o(m_1)$  and  $d_g(p) = \Omega(m_2)$ . The instance admits a solution with a makespan of  $O(d_g(p))$ , computable in  $O(m_1 m_2 d_g(p))$  time.*

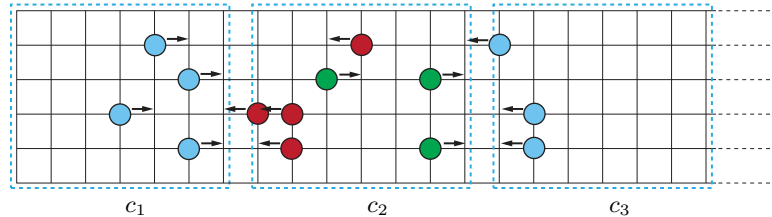


Figure 16: Partitioning of an  $m_1 \times m_2$  grid along the  $m_1$  dimension into  $q = \lfloor m_1/d_g \rfloor$  cells of roughly the same size of  $w \times m_2$  with  $w \approx m_1/q$ . Three partitioned cells  $c_1, c_2$  and  $c_3$  are shown. Four robots need to move from  $c_1$  to  $c_2$  and three robots need to move from  $c_2$  to  $c_3$ . Equal number of robots must move in the opposite direction. The goals of the robots are not illustrated in the drawing.

*Proof.* When  $d_g = \Omega(m_2)$ , We compute  $q = \lfloor m_1/d_g \rfloor$  and  $w = \lfloor m_1/q \rfloor$  (note that  $w \geq d_g$ ). Partition  $G$  into  $q$  grid cells along the direction of  $m_1$ ; each cell is of size  $m_2 \times w$  or  $m_2 \times (w+1)$  (see Fig. 16). Assuming that

$G$  is oriented such that its longer dimension is aligned horizontally, then from left to right, we label these cells  $c_1, \dots, c_q$ . By the definition of  $d_g$ , a robot initially located in cell  $c_i$  may only have its goal in either  $c_{i-1}$ ,  $c_i$ , or  $c_{i+1}$  (for applicable  $i-1$ , and  $i+1$ ). This further implies that for any applicable  $i$ , the number of robots that needs to move from  $c_i$  to  $c_{i+1}$  is the same as the number of robots that needs to move from  $c_{i+1}$  to  $c_i$ . The MPP instance can then be solved in two rounds through first invoking iSAG on the combined cells  $c_i + c_{i+1}$  for all applicable odd  $i$ . This round finishes all robot exchanges between  $c_i$  and  $c_{i+1}$  for odd  $i$ . In the second round, iSAG is invoked again to do the same, now for all applicable even  $i$ . Since both parallel applications of iSAG incur a makespan of  $O(w + d_g) = O(d_g)$ , the total makespan is  $O(d_g)$ . For running time, each round of iSAG application requires  $O(q(d_g^2 m_2 + d_g m_2^2))$ . Since  $q = O(\frac{m_1}{d_g})$  and  $d_g = \Omega(m_2)$ , this yields a total time of  $O(m_1 m_2 d_g)$ .  $\square$

The rest of this section is devoted to the case  $d_g = o(m_2)$ . Because  $d_g = o(m_2)$ , without loss of generality, we assume that  $m_1 \geq m_2 \geq 5d_g$ . Furthermore, we may assume without loss of generality that  $m_1$  and  $m_2$  are multiples of  $5d_g$ . If that is not the case, assuming that PAF is correct, then we can apply PAF up to four times without adding makespan or running time penalty. To execute this, first we compute  $q_1 = \lfloor m_1 / (5d_g) \rfloor$  and  $q_2 = \lfloor m_2 / (5d_g) \rfloor$ . We note that  $|V| \approx q_1 q_2 d_g^2$ . Then, PAF is applied to the top left portion of  $G$ . This will fully solve the problem for the top left  $(q_1 - 1) \times (q_2 - 1)$  cells of sizes  $5d_g \times 5d_g$ . Doing the same three more times with each application on a different section of  $G$ , as illustrated in Fig. 17, the entire problem is then solved.

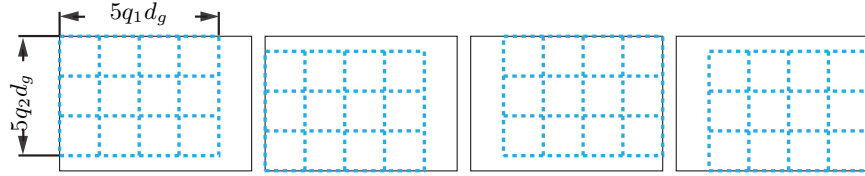


Figure 17: For  $G = m_1 \times m_2$ , if  $m_1$  or  $m_2$  are not multiples of  $5d_g$ , we may apply PAF to a  $q_1 \times q_2$  cell partition of  $G$  up to four times to cover  $G$ .

Henceforth in this section, we assume  $m_1 = 5q_1 d_g$  and  $m_2 = 5q_2 d_g$  in which  $q_1$  and  $q_2$  are integers.  $G$  is partitioned into a  $q_1 \times q_2$  *skeleton grid*  $G_S$  with its nodes being  $5d_g \times 5d_g$  cells. We remind the readers that after the partition, by the definition of  $d_g$ , robot exchanges between cells can only happen in a  $d_g$  wide border for any cell, as explained earlier and illustrated in Fig. 12. Our immediate goal is to make sure that between neighboring cells, the movement of robots are uni-directional and does not happen between diagonally adjacent cells. That is, we would like to realize what is illustrated in Fig. 15(a) from a raw partition, in polynomial time and  $O(d_g)$  makespan, using *diagonal rerouting* (Fig. 13) and *flow cancellation* (Fig. 14) operations.

**Lemma 12** (Flow Orientation). *In  $O(m_1 m_2 d_g)$  time and  $O(d_g)$  makespan, the flow of robots on the  $q_1 \times q_2$  skeleton grid may be arranged to be only vertical or horizontal between adjacent cells and uni-directional. The largest total incoming flow through a cell boundary is no more than  $6d_g^2$ .*

*Proof.* We first show how to carry out the diagonal rerouting operation. For convenience and with more details, we reproduce Fig. 13 in Fig. 18 and let the four involved cells be  $c_1$  through  $c_4$  as illustrated. By the definition of  $d_g$ , if a robot 1 in  $c_1$  has its goal in  $c_3$ , then the robot must be in the bottom right  $d_g \times d_g$  region of  $c_1$  and its goal must be in the top left  $d_g \times d_g$  region of  $c_3$ . For each such robot, we pick an arbitrary robot 2 from  $c_2$  in the diagonal-line shaded region. Any robot in this region will have its goal in  $c_2$  (by definition of  $d_g$ ). If we swap the initial configurations of 1 and 2, then the diagonal movement of 1 is eliminated. Going in a clockwise fashion, for any robot in  $c_2$  that needs to move to  $c_4$ , we can swap it with a robot from  $c_3$  in the diagonal-line shaded region. Within the  $4d_g \times 4d_g$  region, we create a (temporary) MPP problem containing only these swaps. For each such meetings of four cells, such an MPP instance is created. Then, all these disjoint instances can be solved with iSAG in parallel using only  $O(d_g)$  makespan. For computation time, constructing the instance requires a single linear scan of the  $4d_g \times 4d_g$  region and solving each MPP

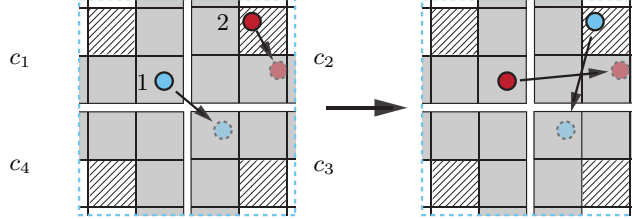


Figure 18: Illustration of four cells meeting at corners. Each small square region is of size  $d_g \times d_g$ . The entire region is of size  $4d_g \times 4d_g$ . Swapping 1 and 2 eliminates the need for 1 to directly cross into a diagonally adjacent cell.

instance takes  $(16d_g^2)^{\frac{3}{2}} = O(d_g^3)$  time, by Corollary 8. There are  $q_1 q_2$  such instances, demanding a total time of  $O(q_1 q_2 d_g^3) = O(m_1 m_2 d_g)$ .

The flow cancellation operation is carried out using a mechanism similar to that for diagonal rerouting. Referring to Fig. 19 as an updated version of Fig. 14(a), for a horizontal boundary between two adjacent cells  $c_1$  and  $c_2$ , there can be robots that are more than  $d_g$  away from the boundary that need to cross the boundary. This is due to the diagonal rerouting step. Suppose that there are  $n_1$  robots that need to move from  $c_1$  to  $c_2$  and  $n_2$  from  $c_2$  to  $c_1$ . We may pick  $\min\{n_1, n_2\}$  robots from each group and create an MPP problem that swap them on the  $5d_g \times 4d_g$  region as shown in Fig. 19. Applying iSAG on the instance

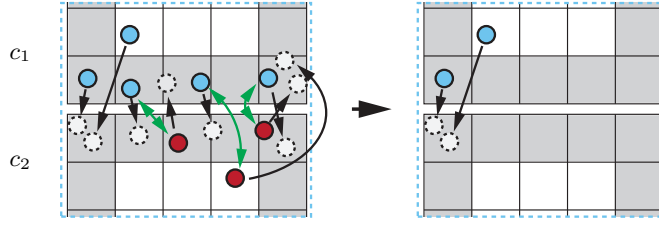


Figure 19: A horizontal boundary between two adjacent cells. Some potential robot movements across the boundary are illustrated. Among these, three pairs of robots, as indicated with double sided arrows, may be matched to make the flow across the boundary uni-directional.

then renders the flow of robots between the boundary uni-directional. By applying iSAG in parallel on all such instances over horizontal boundaries and then another round over vertical boundaries, flows of robots between cell boundaries are all uni-directional. Following the analysis of diagonal rerouting step, the flow cancellation operation also induces  $O(d_g)$  makespan because each MPP instance is on an  $O(d_g) \times O(d_g)$  grid region. The running time is also the same as the diagonal rerouting step at  $O(m_1 m_2 d_g)$ . It is clear that the total flow through any boundary is no more than  $5d_g^2 + d_g^2/2 + d_g^2/2 = 6d_g^2$ .  $\square$

After the flow cancellation operation, we are left with only unidirectional flows on the skeleton grid  $G_S$  that are either vertical or horizontal between adjacent cells. To route the robots these flows represent, closed disjoint cycles must be constructed for moving the robots synchronously across multiple cell boundaries. To achieve this, we will first decompose the flow into unit circulations (i.e., describing a procedure for going from Fig. 15(a) to Fig. 15(b)). Then, we will show how the cycles on the skeleton grid  $G_S$  (e.g., Fig. 15(b)) can be grouped into a constant number of  $d_g^2$  sized batches and turned into actual cycles on the original grid  $G$ . Our flow decomposition result, outlined below, works for arbitrary graphs.

**Theorem 13** (Circulation Decomposition). *Let  $\mathcal{C}$  be a circulation on a graph  $G = (V, E)$  with the largest total incoming flow for any vertex being  $f > 0$ .  $\mathcal{C}$  can be decomposed into  $f$  unit circulations on  $G$  in  $O(f^2|V|)$  time or  $O(f|V|\log|V|)$  expected time.*

*Proof.* We proceed to build a bipartite graph over two copies of  $|V|$ . For a vertex  $v_i \in V$ , we denote one of the copy  $v_i^1$  (belonging to the first partite set) and the other  $v_i^2$  (belonging to the second partite set). For

any two adjacent vertices  $v_i, v_j \in V$ , if there is a flow of magnitude  $f_{ij}$  from  $v_i$  to  $v_j$ , then we add  $f_{ij}$  edges between  $v_i^1$  and  $v_j^2$ . Because the largest total incoming flow to any vertex is  $f$ , the maximum degree for any  $v_i^j$ ,  $j = 1, 2$ , is also  $f$ . Also, due to flow conservation at vertices, for fixed  $v_i \in V$ ,  $v_i^1$  and  $v_i^2$  have the same degree  $f_i \leq f$ . For all  $v_i$  with  $f_i < f$ , we add  $f - f_i$  edges between  $v_i^1$  and  $v_i^2$ . This brings the degrees of all vertices in the bipartite graph to  $f$ , yielding a regular bipartite graph. The bipartite graph has  $2|V|$  vertices and  $f|V|$  edges. An illustration of the bipartite graph construction is given in Fig. 20.

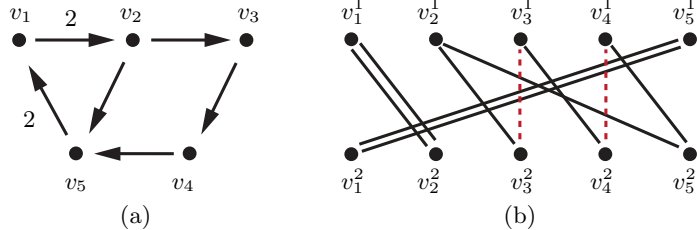


Figure 20: (a) A graph with five vertices and a valid circulation of largest total incoming degree being 2. The flow on each edge with non-unit flow is marked on the edge. (b) The constructed bipartite graph. The dashed edges are the edges added to make the graph regular.

With the regular bipartite graph of degree  $f$ , by Hall's theorem [49], there exists a perfect matching that can be computed in  $O(|E|) = O(f|V|)$  time [52]. The matching corresponds to a unit circulation on  $G$ , which translates to either a single cycle or multiple vertex disjoint cycles. In the example, a perfect matching may be  $(v_1^1, v_2^2), (v_2^1, v_5^2), (v_3^1, v_3^2), (v_4^1, v_4^2), (v_5^2, v_1^1)$ , which translates to the cycle  $v_1v_2v_5v_1$ . An application of the perfect matching algorithm reduces the degree of the bipartite graph by 1, resulting in another regular bipartite graph. We may repeat the procedure  $f$  times to obtain  $f$  unit circulations on  $G$ . The total running time to obtain the  $f$  unit circulations is  $O(f^2|V|)$ . Alternatively, we may use the randomized  $O(|V| \log |V|)$  perfect matching algorithm [53], which yields a total expected running time of  $O(f|V| \log |V|) = \tilde{O}(f|V|)$ .  $\square$

For our setting, Theorem 13 implies the following (note that  $|V| = O(q_1 q_2)$  and  $f = O(d_g^2)$ .)

**Corollary 14** (Flow Decomposition on Skeleton Grid). *An  $O(d_g^2)$  circulation on a  $q_1 \times q_2$  skeleton grid can be decomposed into  $O(d_g^2)$  unit circulations in  $O(m_1 m_2 d_g^2)$  time or  $O(m_1 m_2 \log \frac{m_1 m_2}{d_g^2})$  expected time.*

Because at most  $6d_g^2$  flows can pass through a cell boundary, at most  $12d_g^2$  flow can pass through a cell (two incoming, two outgoing). Corollary 14 gives us  $12d_g^2$  unit circulations over the skeleton grid  $G_S$ . With the decomposed circulation, we may group them into batches and translate these into actual robot movements on  $G$ . To start, we handle a  $d_g$  batch.

**Lemma 15** (Single Batch Global Flow Routing). *A batch of up to  $d_g$  unit circulations on the  $q_1 \times q_2$  skeleton grid may be translated into actual cyclic paths for robots on  $G$  to complete in a single step, using  $O(m_1 m_2)$  time.*

*Proof.* For a fixed cell, there are many possible orientations for the incoming and outgoing flows. However, we only need to analyze the case where all four boundaries of a cell have flows passing through. If we can handle these, other cases are degenerate ones with some flows crossing the boundaries being zero. Among all possible flows that go through all sides of a cell, there are only three possible orientations for the incoming and outgoing flows after considering rotation symmetries and flow direction symmetries, as illustrated in Fig. 21. For example, the case with one incoming flow and three outgoing flows is the same as reversing the directions of the arrows in the case shown in Fig. 21(a). Therefore, establishing how a  $d_g$  amount of flow may be translated into feasible robot movements for the three cases in Fig. 21 encompasses all possible scenarios. We will establish how up to  $d_g$  robots can be arranged to go through the boundaries in a single step for all three cases.

To route the robots, we will only use the center “+” area of  $d_g$  width of each  $5d_g \times 5d_g$  cell. Fig. 22 illustrates the routing plan for realizing the flow given in Fig. 21(a), which may be readily verified to be correct using basic algebra (i.e., assuming the top, left, and bottom routes contain  $x, y$ , and  $z$  flows, respectively, such that  $x + y + z \leq d_g$ ); we omit the inclusion of the straightforward argument here. For arranging the

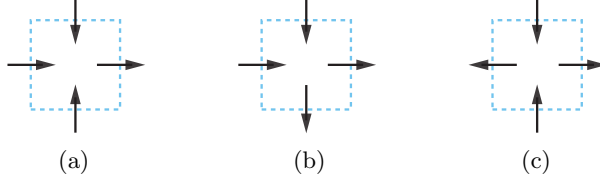


Figure 21: Three possible flow orientations that cover all possible cases considering flow quantity (which may be zero) and symmetries (flipping of all flow directions and rotating the cell).

robots, for horizontal cell boundaries, robots are aligned left. For vertical boundaries, robots are aligned toward the top. We note that if Fig. 21(a) is rotated, some adjustments are needed due to this choice of robot alignment but the change is minimal. Such alignments are necessary to ensure that the robot movements at cell boundaries match.

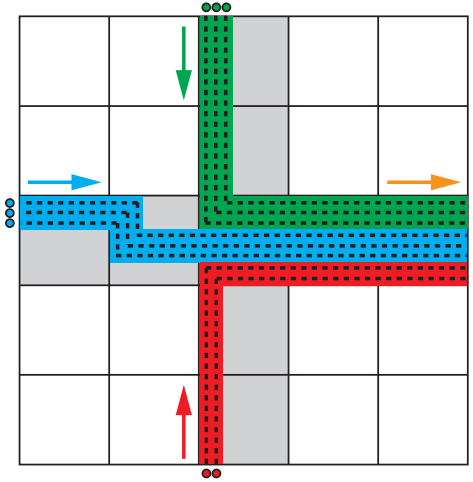


Figure 22: Illustration of how a flow of size 8 may be translated to plans for robots for the case shown in Fig. 21(a). Each small square is of size  $d_g \times d_g$ .

It is important to emphasize that we construct the paths so that for the incoming and outgoing  $d_g \times d_g$  boundary areas of the “+” that are involved, robots only move straight through it, which is not necessary but simplifies things when we put multiple batches together later. For the cases from Fig. 21(b) and (c), illustrations of feasible routing plan construction are given in Fig. 23. Again, the incoming and outgoing flows follow straight lines in the  $d_g \times d_g$  boundary areas of the “+” region. Because at most a  $d_g$  amount of flow is being handled at a time per cell, the incoming flows can always be aggregated into the center  $d_g \times d_g$  area before they get distributed outward to exit the cell.

Because there are only a constant number of flow arrangements for a cell (e.g., the three cases from Fig. 21 plus some symmetric variants), there are only a constant number of possible parametrized routing plans. To compute such a plan, we note that each path is specified by a constant number of parameters. Together, this implies that the construction of the required paths for routing the robots in each cell only require a single pass through the cell, doable in  $O(d_g^2)$  time. For  $q_1 q_2$  cells, the total is  $O(q_1 q_2 d_g^2) = O(m_1 m_2) = O(|V|)$ .  $\square$

With a subroutine to push through  $G$  a batch of up to  $d_g$  unit circulations each step,  $d_g$  such batches may be further grouped for sequential execution, allowing the handling of up to  $d_g^2$  at a time. This is established in the following lemma.

**Lemma 16** (Multi-Batch Global Flow Routing). *Up to  $d_g^2$  unit circulations on the  $q_1 \times q_2$  skeleton grid can be routed through  $G$  using  $O(d_g)$  makespan and  $O(m_1 m_2 d_g)$  time.*

*Proof.* For the proof, we only need to focus on a single  $d_g \times d_g$  boundary area of a single cell; all other boundaries and cells will be handled similarly. Moreover, we only need to worry about robots moving out

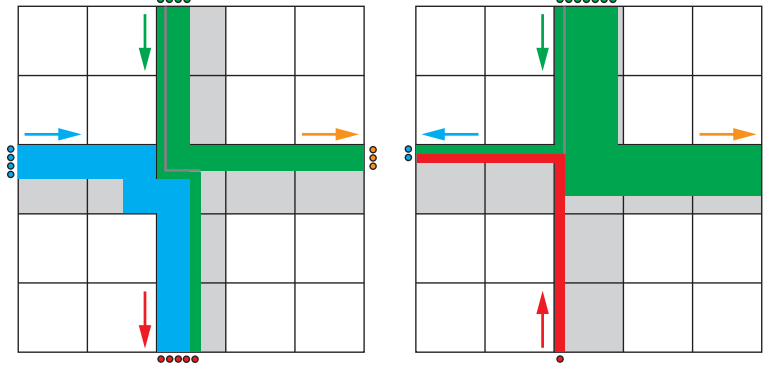


Figure 23: Illustration of how flows be translated into feasible robot movements for the cases in Fig. 21, (b) and (c), respectively. Each small square is of size  $d_g \times d_g$ . Because the incoming flows add up to no more than  $d_g$ , it is always possible to aggregate them into the center  $d_g \times d_g$  area before sending them out of the cell.

of a cell due to symmetry. With these reductions, we outline how to push up to  $d_g^2$  robots out of the right boundary of the “+” region of a cell, which is a  $d_g \times d_g$  grid. Call this  $d_g \times d_g$  grid  $c$ . After dicing up the  $d_g^2$  circulations into  $d_g$  of  $d_g$  sized batches, we invoke Lemma 15 to generate feasible routing plans for each  $d_g$  sized batch. Because Lemma 15 guarantees that the generated paths are straight lines from left to right inside  $c$ , these batches can be sequentially arranged one after another for execution. An example for  $d_g = 6$  is illustrated in Fig. 24 with each color representing a  $d_g$  sized batch to be moved out through the right in one step. It is straightforward to check that the batches, when arranged into configurations as illustrated in Fig. 24(c), can be readily executed sequentially. In particular, once the paths for earlier batches are completed, the execution itself also prepares the next batch for execution (see Fig. 25).

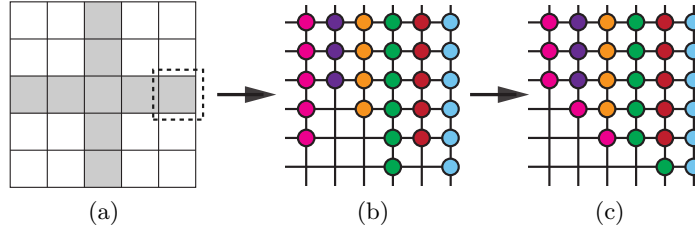


Figure 24: (a) We are to route  $d_g^2$  circulations through the right boundary of a cell in a  $d_g \times d_g$  area, highlighted with the dashed square. (b) The plans generated for the  $d_g$  of  $d_g$  sized batches are arranged so that earlier plans appear on the right. For later plans, part of it get truncated. (c) The further compacted batches for actual execution. For robots that are not shown, they will stay in the cell and have no impact on the plan execution.

For computation time, for the  $d_g^2$  circulation, we need to invoke the procedure from Lemma 15 for all  $q_1 q_2$  cells  $d_g$  times, which incur a cost of  $O(q_1 q_2 d_g^3) = O(m_1 m_2 d_g)$  running time, mostly used to write down the paths. To be able to actually prepare a cell for execution, iSAG must be invoked on the cell once, which takes  $O(m_1 m_2 d_g)$  time over all cells. This is the dominating term.  $\square$

We will now complete proving Theorem 10.

*Proof of Theorem 10.* For the case of  $d_g = o(m_2)$ , on a  $q_1 \times q_2$  skeleton grid  $G_S$  with each node being a  $5d_g \times 5d_g$  cell, we first apply Lemma 12 to ensure that flows of robots across cell boundaries are uni-direction without diagonal movements, in  $O(m_1 m_2 d_g)$  time. Then, Corollary 14 computes a decomposition of the flow into up to  $12d_g^2$  (vertex) unit circulations, in  $O(m_1 m_2 d_g^2)$  time. Invoking Lemma 16 a constant number of times, in  $O(m_1 m_2 d_g)$  running time, we may globally route the robots so that all robots will be in the cell where its goal belongs to. We are then left with solving an MPP for each individual cell, which again requires  $O(m_1 m_2 d_g)$  running time over all cells. Putting this together with the cases handled by Lemma 11,

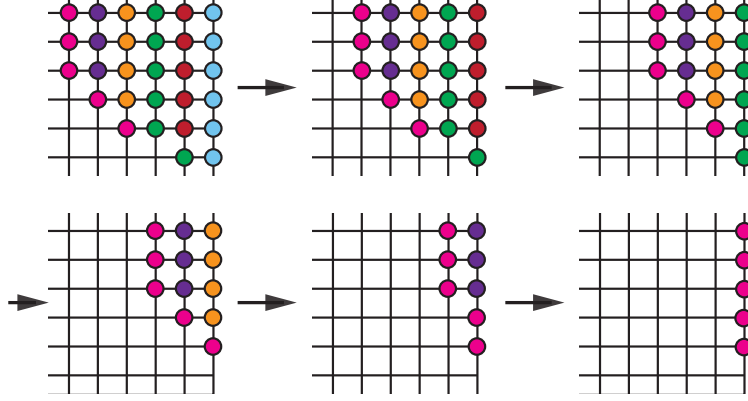


Figure 25: Illustration of sequential execution of  $d_g = 6$   $d_g$  sized batches.

we concluded that an MPP instance can be solved with  $O(d_g)$  makespan in  $O(m_1 m_2 d_g^2)$  time. If we use the randomized algorithm [53] for matching, then the running time becomes  $O(m_1 m_2 d_g + m_1 m_2 \log \frac{m_1 m_2}{d_g^2})$  expected time.  $\square$

Due to the dimension ignorant flow decomposition algorithm (Theorem 13), the running time for PAF in two dimensions incurs some additional cost over the comparable algorithm from [2]. On the other hand, the more general decomposition, coupled with iSAG which directly supports arbitrary dimensions, enables the extension of PAF to three dimensions.

## 6 PartitionAndFlow in Three Dimensions

It is clear that the overall PAF strategy for two dimensions generalizes to arbitrary dimensions except when it comes to turn the decomposed flows into actually routing plan. We show how this can be done for three dimensions. On an  $m_1 \times m_2 \times m_3$  grid, we focus on the main case of  $d_g = o(m_3)$ . For 3D, we will use a partition of cells of sizes  $9d_g \times 9d_g \times 9d_g$  and assume that  $9d_g$  divides  $m_i$ , i.e.,  $m_i = q_i 9d_g, 1 \leq i \leq 3$ . It is straightforward to verify that PAF in 2D carries over except it is not clear how to route  $d_g^3$  flow through the faces of a  $9d_g \times 9d_g \times 9d_g$  cell, which requires the routing of  $d_g^2$  flow in a single step. Generating paths for routing robots corresponding to the flow is significantly more involved than in the 2D case. First, we match the up to six incoming and outgoing flows through a single cell so that at most one face sends flow to its opposite face. If there is a single pair of opposite faces with one having incoming flow and one having outgoing flow, nothing needs to be done. Otherwise, if there are multiple such face pairs, pick two arbitrary such pairs  $a_1, a_2, b_1$ , and  $b_2$ . Without loss of generality, assume  $f_{a_1} > 0, f_{a_2} < 0, f_{b_1} > 0$ , and  $f_{b_2} < 0$  (this is similar to the case illustrated in Fig. 21(b)). If  $f_{a_1} \leq |f_{b_2}|$ , then we route all  $f_{a_1}$  flow into  $a_1$  to go out through  $b_2$ , which then avoids the need for routing any flow into  $a_1$  to go out from  $a_2$ . If  $f_{a_1} > |f_{b_2}|$ , we do the same, which means that no flow from  $b_1$  needs to go out through  $b_2$ . Either way, we effectively get rid of a dimension  $i$  where  $f_{i_1} * f_{i_2} < 0$ . Doing this iteratively then leaves at most one such dimension where we may need to route any flow between the two opposite faces associated with that dimension.

We now show how we may route flow from one face to other five faces through a  $9d_g \times 9d_g \times 9d_g$  cell. Without loss of generality, we will show how to route flow coming in from the top face to the right face. Routing to the opposite face will be briefly explained afterward. We will route the flow to go through the center  $d_g \times d_g$  regions on the six faces of the  $9d_g \times 9d_g \times 9d_g$  cell and assume that a protocol is agreed on how the flow will be *shaped* between difference cells so the robot flows can be matched at cell boundaries. For example, on the top face, the  $d_g^2$  flow may be ordered row by row (e.g., the 24 robots on the top of Fig. 27(a)), which result in a contiguous 2D shape inside a  $d_g \times d_g$  region. Depending on the flow routing plan, this up to  $d_g^2$  amount of flow is partitioned into 5 pieces (left, right, front, back, and center). We note that these pieces can again be made contiguous and in particular do not *interlock* with each other (bottom

of Fig. 27(a)). Based on the partition, the proper amount of flow to each face is then *pivoted* to go sideways row by row (see left figure of Fig. 27(b)), except for flow that goes to the opposite face.

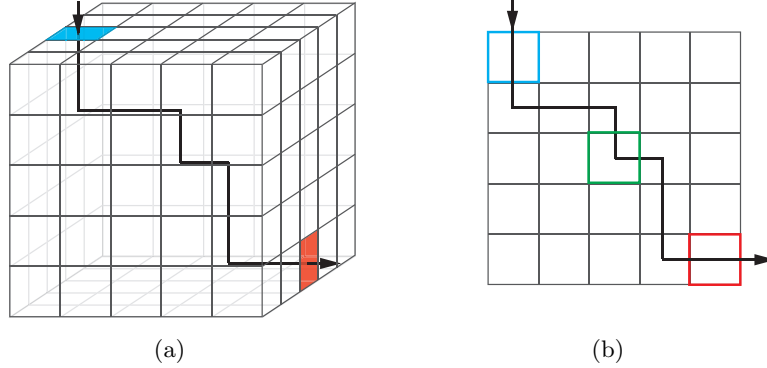


Figure 26: Illustration of how a certain amount of flow may be routed sideways. Only the top-right-middle  $5d_g \times 5d_g \times 5d_g$  portion of the cell is shown in (a). (b) is a projective view from the front.

For the flow going to the right face, we rearrange them to a row-majorized shape using a  $2d_g \times d_g \times d_g$  grid, as illustrated in Fig. 27(b). At this point, we note that by symmetry, the same procedure can be applied to the flow going out of the right face in the reverse direction. Using a  $d_g \times d_g \times d_g$  grid (the green one in Fig. 26(b) and Fig. 27(b)) as a buffer zone, these two separately crafted routes can be perfectly matched, completing the routing plan for a pair of faces. For routing flow to an opposite face, we simply let the flow to go down two more  $d_g \times d_g \times d_g$  grids after going through the blue  $d_g \times d_g \times d_g$  grid, after which we can do the same reshaping procedure. Once we can route  $d_g^2$  flow through using a single step, we can do  $d_g$  batches of these, pushing  $d_g^3$  flow in  $O(d_g)$  makespan.

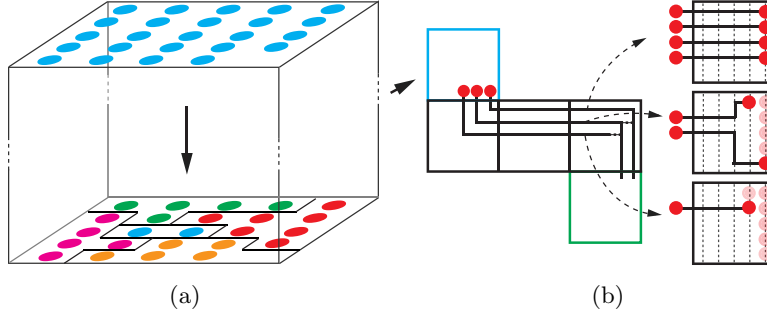


Figure 27: (a) Incoming  $d_g^2$  flow may be broken into non-interlocking pieces going to different faces. This  $d_g \times d_g \times d_g$  grid corresponds to the cyan topped grid in Fig. 26(a). (b) A projective view (from the front) of how the three rows of red robots can be routed and reshaped into two row-major ordered rows, going downwards.

Our main goal so far is to show that it is feasible to route  $d_g^3$  flow in  $O(d_g)$  make span. To actually create the routing plan, we apply the max-flow algorithm (e.g., [54]) to an augmented direct graph generated on the  $9d_g \times 9d_g \times 9d_g$  grid via vertex splitting, a standard technique used in finding vertex disjoint paths. We summarize the results in the following theorem.

**Theorem 17** (PAF in Three Dimensions). *Let  $G = (V, E)$  be an  $m_1 \times m_2 \times m_3$  grid. Let  $p$  be an arbitrary MPP instance on  $G$ . A solution with  $O(d_g(p))$  makespan can be computed in  $O(d_g^3|V|)$  and  $O(|V|^2)$  time.*

*Proof.* Without loss of generality, we may assume that  $m_1, m_2$ , and  $m_3$  are desired multiples of  $d_g$  as needed.

For  $k = 3$ ,  $d_g$ , when compared with  $m_1, m_2$ , and  $m_3$  (we remind the reader that  $m_1 \geq m_2 \geq m_3$  and we assume  $d_g = o(m_1)$ ), raises three cases: (i)  $d_g = o(m_1)$  and  $d_g = \Omega(m_2)$ , (ii)  $d_g = o(m_2)$  and  $d_g = \Omega(m_3)$ , and (iii)  $d_g = o(m_3)$ . We note that  $O(d_g^3|V|)$  and  $o(|V|^2)$  do not necessarily imply each other in all cases.

For the case of  $d_g = o(m_1)$  and  $d_g = \Omega(m_2)$ , a result similar to Lemma 11 can be proved, over a partition of  $G$  as illustrated in Fig. 28. The overall makespan is readily verified as  $O(d_g)$ . The only difference, as compared with the proof for Lemma 11, is that the 3D version of iSAG needs to be used. By Theorem 7,

solving a single 3D iSAG on a  $d_g \times m_2 \times m_3$  grid takes time  $O(d_g^2 m_2 m_3 + d_g m_2^2 m_3 + d_g m_2 m_3^2)$ . Making a total  $\frac{m_1}{d_g}$  of such parallel calls takes time  $O(d_g m_1 m_2 m_3) = O(d_g |V|)$ , which is both  $O(d_g^3 |V|)$  and  $o(|V|^2)$ .

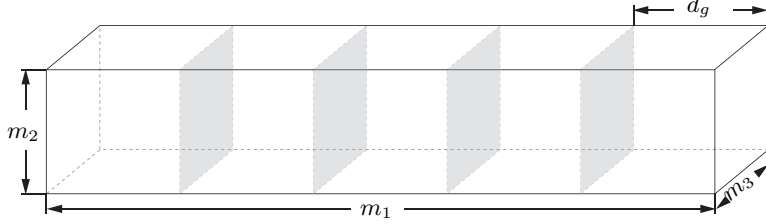


Figure 28: In the case of  $d_g = o(m_1)$  and  $d_g = \Omega(m_2)$ ,  $G$  may be partitioned blocks of size  $d_g \times m_2 \times m_3$ .

For the case of  $d_g = o(m_2)$  and  $d_g = \Omega(m_3)$ , we partition  $G$  into cells of size  $5d_g \times 5d_g \times m_3$  each, as illustrated in Fig. 29, to get a  $q_1 \times q_2$  2D skeleton grid  $G_S$  of these cells. For solving the partitioned problem, we essentially follow the main case of PAF in 2D. The procedures for carrying out diagonal rerouting and flow cancellation (Lemma 12) can be executed as is on  $G_S$  using 3D iSAG. For flow decomposition on  $G_S$ , instead of up to  $6d_g^2$  flow, the 3D case now has up to  $6m_3 d_g^2$  flow through a cell boundary. The same flow decomposition procedure (i.e., Corollary 14) can nevertheless be carried out to decompose  $O(m_3 d_g^2)$  flow on  $G_S$  into unit circulations, as  $O(d_g)$  of  $m_3 d_g$  sized batches. This is because the boundary between two cells is now a  $d_g \times m_3$  2D grid and can allow  $m_3 d_g$  robots to pass through at a single step. The conversion of the flow into executable paths for global robot routing can then be completed using the 3D extended version of Lemma 15 and Lemma 16; adding a dimension orthogonal to the  $d_g \times d_g$  grid is straightforward. After the global routing step, each robot resides in a cell where its goal also resides; a parallel call to 3D iSAG on all individual cells then solves the problem.

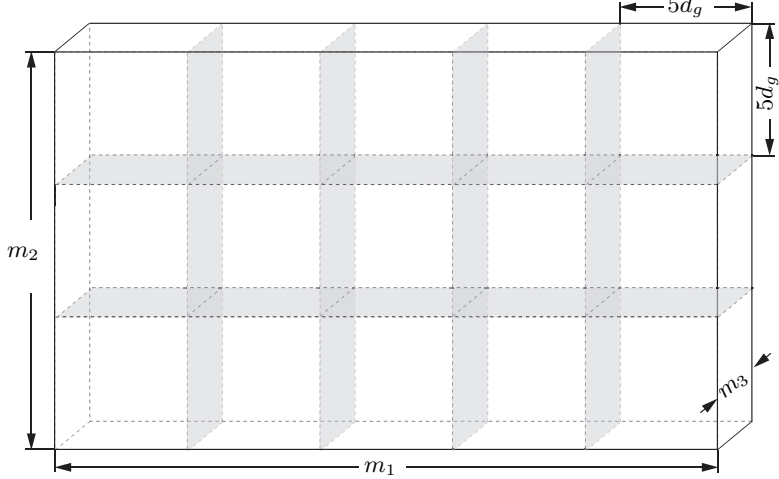


Figure 29: In the case of  $d_g = o(m_2)$  and  $d_g = \Omega(m_3)$ ,  $G$  may be partitioned into blocks of size  $5d_g \times 5d_g \times m_3$ .

Again, the resulting makespan for this case is clearly  $O(d_g)$ . Running time wise, the flow decomposition needs to route  $f = O(m_3 d_g^2)$  flow on a skeleton grid with  $\frac{m_1 m_2}{d_g^2}$  edges, which requires a total running time of  $O(m_1 m_2 m_3^2 d_g^2)$ . The other cost is to invoke 3D iSAG in parallel on  $\frac{m_1 m_2}{d_g^2}$  of  $5d_g \times 5d_g \times m_3$  sized cells, which by Theorem 7 takes time  $O(\frac{m_1 m_2}{d_g^2} (d_g^3 m_3 + d_g^3 m_3 + d_g^2 m_3^2)) = O(d_g m_1 m_2 m_3)$ . The overall running time is then  $O(d_g^2 m_1 m_2 m_3^2)$ . Because  $d_g = o(m_2)$  and  $d_g = \Omega(m_3)$ , the running time is both  $O(d_g^3 |V|)$  and  $o(|V|^2)$ .

For the main case of  $d_g = o(m_3)$ , we partition  $G$  into  $9d_g \times 9d_g \times 9d_g$  cells. Assuming  $m_1 = 9q_1 g_d$ ,  $m_2 = 9q_2 g_d$ , and  $m_3 = 9q_3 g_d$ , this yields a 3D skeleton grid  $G_S$  of dimensions  $q_1 \times q_2 \times q_3$  (we omit the pictorial illustration of the case, which is difficult to visually observe). In this case, each cell  $c$  may interface with 26 other cells, with 6 of these neighbors each sharing a  $9d_g \times 9d_g$  boundary with  $c$ . The rest 20 neighbors of  $c$

are diagonal neighbors of some form, either along a  $9d_g$  length edge (12 of these, denoted as edge-diagonal neighbors) or a single vertex (8 of these, denoted as vertex-diagonal neighbors).

For the main case, we verify that the flow orientations steps (Lemma 12) carry over with minor modifications: more calls to iSAG is required for each cell due to the increased number of neighbors and 3D diagonal rerouting needs to first convert vertex-diagonals to edge-diagonals. The number of such parallel calls to iSAG remains constant, however, retaining the  $O(d_g)$  makespan guarantee and actually reduces the asymptotic running time. The flow decomposition step (Corollary 14) extends with the flow amount being  $O(d_g^3)$  per cell, decomposed into  $O(d_g)$  of  $d_g^2$  sized batches.

To construct a global routing plan for realizing these batches, instead of using manual construction as we have done with Lemma 15 and Lemma 16, in the 2D case, we directly apply max-flow to generate the vertex disjoint paths for routing the robots. After the flow decomposition step, each batch of up to  $d_g^2$  flow, by our earlier argument, is always possible to be routed through a  $9d_g \times 9d_g \times 9d_g$  cell. We may invoke the Ford-Fulkerson algorithm [54] on an auxiliary graph (through vertex splitting, a standard technique) of the  $9d_g \times 9d_g \times 9d_g$  cell to obtain up to  $d_g^2$  vertex disjoint paths, which route that many robots in a single step through the cell. It is possible to bundle  $d_g$  of  $d_g^2$  sized batches together, which incur a makespan of  $d_g$ . Therefore, similar to the 2D case, the global robot routing can be completed using  $O(d_g)$  makespan.

With the global routing of robots completed, we again end up with the case that every robot is now in a cell where its goal also belongs to. iSAG can then be invoked to solve the problem in parallel. Following similar analysis as in the 2D case, the algorithm produces an  $O(d_g)$  makespan solution. For running time, there are three main costs: (i) iSAG calls, (ii) matching for flow decomposition, and (iii) max-flow based global robot routing plan generation. For (i),  $q_1 q_2 q_3$  parallel calls to 3D iSAG is needed, demanding a time of  $O(q_1 q_2 q_3 d_g^4) = O(d_g |V|)$ . For (ii), flow decomposition is now performed on  $O(d_g^3)$  flow on a graph with  $O(q_1 q_2 q_3 d_g^3)$  edges, requiring  $O(d_g^3 |V|)$  time. For (iii), using Ford-Fulkerson [54], the total running time is  $O(q_1 q_2 q_3 d_g^6) = O(d_g^3 |V|)$ , which is  $o(|V|^2)$ .  $\square$

## 7 Discussion

We conclude the paper discussing some natural extensions of iSAG and PAF.

*Extension to other grid-like graphs.* Our results have focused on the underlying graph  $G$  being axis-aligned grids. As pointed out in [1], the results developed in this paper readily apply to other types of grid-like graphs, e.g., honeycombs and grids with triangular faces. Indeed, as long as the graph admits some forms of Lemma 2 and Lemma 3, then a version of iSAG can be derived for the setting. For the decomposed global flow to be routed effectively, some form of feasibility argument is needed, which can be ensured if the underlying graph can be partitioned into orthogonal dimensions.

*Continuous domain.* As pointed out in [1] and with more details in [2,55], routing algorithms on grids also extend to continuous settings for the routing of identical sized disc robots (balls in higher dimensions) that may be packed arbitrarily close to each other. The extension is carried out with an expansion phase of the (continuous) initial configuration such that sufficient space is available for aligning the robots, as unlabeled ones, onto a grid for routing. This yields a grid  $G$  and an associated  $X_I$ . The same is applied to the goal configuration, which will use the same  $G$  and produces an  $X_G$ . Since the expansion only needs to grow volume occupied by the initial configuration by a constant (for fixed dimension  $k$ ), the  $O(1)$ -approximation guarantee is then fully preserved.

**Acknowledgments.** The author would like to thank Pranjal Awasthi and Mario Szegedy for helpful discussions.

## References

- [1] J. Yu, “Average case constant factor optimal multi-robot path planning in well-connected environments,” *arXiv preprint arXiv:1706.07255*, 2017, note: A preliminary version appeared in the First International Symposium on Multi-Robot and Multi-Agent Systems, 2017.
- [2] E. D. Demaine, S. P. Fekete, P. Keldenich, H. Meijer, and C. Scheffer, “Coordinated motion planning: Reconfiguring a swarm of labeled robots with bounded stretch,” *arXiv preprint arXiv:1801.01689*, 2018.

- [3] P. R. Wurman, R. D’Andrea, and M. Mountz, “Coordinating hundreds of cooperative, autonomous vehicles in warehouses,” *AI Magazine*, vol. 29, no. 1, pp. 9–19, 2008.
- [4] R. Stahlbock and S. Voß, “Operations research at container terminals: a literature update,” *OR spectrum*, vol. 30, no. 1, pp. 1–52, 2008.
- [5] S. Tang, J. Thomas, and V. Kumar, “Hold or take optimal plan (hoop): A quadratic programming approach to multi-robot trajectory generation,” *The International Journal of Robotics Research*, p. 0278364917741532, 2018.
- [6] M. A. Erdmann and T. Lozano-Pérez, “On multiple moving objects,” in *Proceedings IEEE International Conference on Robotics & Automation*, 1986, pp. 1419–1424.
- [7] S. M. LaValle and S. A. Hutchinson, “Optimal motion planning for multiple robots having independent goals,” *IEEE Transactions on Robotics & Automation*, vol. 14, no. 6, pp. 912–925, Dec. 1998.
- [8] Y. Guo and L. E. Parker, “A distributed and optimal motion planning approach for multiple mobile robots,” in *Proceedings IEEE International Conference on Robotics & Automation*, 2002, pp. 2612–2619.
- [9] R. Jansen and N. Sturtevant, “A new approach to cooperative pathfinding,” in *In International Conference on Autonomous Agents and Multiagent Systems*, 2008, pp. 1401–1404.
- [10] R. Luna and K. E. Bekris, “Push and swap: Fast cooperative path-finding with completeness guarantees,” in *Proceedings International Joint Conference on Artificial Intelligence*, 2011, pp. 294–300.
- [11] T. Standley and R. Korf, “Complete algorithms for cooperative pathfinding problems,” in *Proceedings International Joint Conference on Artificial Intelligence*, 2011, pp. 668–673.
- [12] J. van den Berg, J. Snoeyink, M. Lin, and D. Manocha, “Centralized path planning for multiple robots: Optimal decoupling into sequential plans,” in *Robotics: Science and Systems*, 2009.
- [13] K. Solovey and D. Halperin, “ $k$ -color multi-robot motion planning,” in *Proceedings Workshop on Algorithmic Foundations of Robotics*, 2012.
- [14] J. Yu and S. M. LaValle, “Multi-agent path planning and network flow,” in *Algorithmic Foundations of Robotics X, Springer Tracts in Advanced Robotics*. Springer Berlin/Heidelberg, 2013, vol. 86, pp. 157–173.
- [15] M. Turpin, K. Mohta, N. Michael, and V. Kumar, “CAPT: Concurrent assignment and planning of trajectories for multiple robots,” *International Journal of Robotics Research*, vol. 33, no. 1, pp. 98–112, 2014.
- [16] H. Choset, K. M. Lynch, S. Hutchinson, G. Kantor, W. Burgard, L. E. Kavraki, and S. Thrun, *Principles of Robot Motion: Theory, Algorithms, and Implementations*. Cambridge, MA: MIT Press, 2005.
- [17] J. van den Berg, M. C. Lin, and D. Manocha, “Reciprocal velocity obstacles for real-time multi-agent navigation,” in *Proceedings IEEE International Conference on Robotics & Automation*, 2008, pp. 1928–1935.
- [18] K. E. Bekris, K. I. Tsianos, and L. E. Kavraki, “A decentralized planner that guarantees the safety of communicating vehicles with complex dynamics that replan online,” in *2007 IEEE/RSJ International Conference on Intelligent Robots and Systems*. IEEE, 2007, pp. 3784–3790.
- [19] J. Alonso-Mora, R. Knepper, R. Siegwart, and D. Rus, “Local motion planning for collaborative multi-robot manipulation of deformable objects,” in *2015 IEEE International Conference on Robotics and Automation (ICRA)*. IEEE, 2015, pp. 5495–5502.
- [20] R. A. Knepper and D. Rus, “Pedestrian-inspired sampling-based multi-robot collision avoidance,” in *2012 IEEE RO-MAN: The 21st IEEE International Symposium on Robot and Human Interactive Communication*. IEEE, 2012, pp. 94–100.

- [21] D. Halperin, J.-C. Latombe, and R. Wilson, “A general framework for assembly planning: The motion space approach,” *Algorithmica*, vol. 26, no. 3-4, pp. 577–601, 2000.
- [22] B. Nnaji, *Theory of Automatic Robot Assembly and Programming*. Chapman & Hall, 1992.
- [23] S. Rodriguez and N. M. Amato, “Behavior-based evacuation planning,” in *Proceedings IEEE International Conference on Robotics & Automation*, 2010, pp. 350–355.
- [24] D. Fox, W. Burgard, H. Kruppa, and S. Thrun, “A probabilistic approach to collaborative multi-robot localization,” *Autonomous Robots*, vol. 8, no. 3, pp. 325–344, Jun. 2000.
- [25] J. Ding, K. Chakrabarty, and R. B. Fair, “Scheduling of microfluidic operations for reconfigurable two-dimensional electrowetting arrays,” *IEEE Transactions on Computer-aided Design of Integrated Circuits and Systems*, vol. 20, no. 12, pp. 1463–1468, 2001.
- [26] E. J. Griffith and S. Akella, “Coordinating multiple droplets in planar array digital microfluidic systems,” *International Journal of Robotics Research*, vol. 24, no. 11, pp. 933–949, 2005.
- [27] M. J. Matarić, M. Nilsson, and K. T. Simsarian, “Cooperative multi-robot box pushing,” in *Proceedings IEEE/RSJ International Conference on Intelligent Robots & Systems*, 1995, pp. 556–561.
- [28] D. Rus, B. Donald, and J. Jennings, “Moving furniture with teams of autonomous robots,” in *Proceedings IEEE/RSJ International Conference on Intelligent Robots & Systems*, 1995, pp. 235–242.
- [29] J. S. Jennings, G. Whelan, and W. F. Evans, “Cooperative search and rescue with a team of mobile robots,” in *Proceedings IEEE International Conference on Robotics & Automation*, 1997.
- [30] P. Spirakis and C. K. Yap, “Strong NP-hardness of moving many discs,” *Information Processing Letters*, vol. 19, no. 1, pp. 55–59, 1984.
- [31] J. E. Hopcroft, J. T. Schwartz, and M. Sharir, “On the complexity of motion planning for multiple independent objects; PSPACE-hardness of the “warehouseman’s problem”,” *The International Journal of Robotics Research*, vol. 3, no. 4, pp. 76–88, 1984.
- [32] R. A. Hearn and E. D. Demaine, “PSPACE-completeness of sliding-block puzzles and other problems through the nondeterministic constraint logic model of computation,” *Theoretical Computer Science*, vol. 343, no. 1, pp. 72–96, 2005.
- [33] K. Solovey and D. Halperin, “On the hardness of unlabeled multi-robot motion planning,” in *Robotics: Science and Systems (RSS)*, 2015.
- [34] K. Solovey, J. Yu, O. Zamir, and D. Halperin, “Motion planning for unlabeled discs with optimality guarantees,” in *Robotics: Science and Systems*, 2015.
- [35] D. Kornhauser, G. Miller, and P. Spirakis, “Coordinating pebble motion on graphs, the diameter of permutation groups, and applications,” in *Proceedings IEEE Symposium on Foundations of Computer Science*, 1984, pp. 241–250.
- [36] R. M. Wilson, “Graph puzzles, homotopy, and the alternating group,” *Journal of Combinatorial Theory (B)*, vol. 16, pp. 86–96, 1974.
- [37] V. Auletta, A. Monti, M. Parente, and P. Persiano, “A linear-time algorithm for the feasibility of pebble motion on trees,” *Algorithmica*, vol. 23, pp. 223–245, 1999.
- [38] G. Goraly and R. Hassin, “Multi-color pebble motion on graph,” *Algorithmica*, vol. 58, pp. 610–636, 2010.
- [39] J. Yu and D. Rus, “Pebble motion on graphs with rotations: Efficient feasibility tests and planning,” in *Algorithmic Foundations of Robotics XI, Springer Tracts in Advanced Robotics*, vol. 107. Springer Berlin/Heidelberg, 2015, pp. 729–746.

[40] J. Yu, “Intractability of optimal multi-robot path planning on planar graphs,” *IEEE Robotics and Automation Letters*, vol. 1, no. 1, pp. 33–40, 2016.

[41] G. Sharon, R. Stern, A. Felner, and N. Sturtevant, “Conflict-Based Search for Optimal Multi-Agent Path Finding,” in *Proc of the Twenty-Sixth AAAI Conference on Artificial Intelligence*, 2012.

[42] G. Wagner and H. Choset, “M\*: A complete multirobot path planning algorithm with performance bounds,” in *Proceedings IEEE/RSJ International Conference on Intelligent Robots & Systems*, 2011, pp. 3260–3267.

[43] C. Ferner, G. Wagner, and H. Choset, “Odrm\* optimal multirobot path planning in low dimensional search spaces,” in *Robotics and Automation (ICRA), 2013 IEEE International Conference on*. IEEE, 2013, pp. 3854–3859.

[44] G. Sharon, R. Stern, M. Goldenberg, and A. Felner, “The increasing cost tree search for optimal multi-agent pathfinding,” *Artificial Intelligence*, vol. 195, pp. 470–495, 2013.

[45] E. Boyarski, A. Felner, R. Stern, G. Sharon, O. Betzalel, D. Tolpin, and E. Shimony, “Icbs: The improved conflict-based search algorithm for multi-agent pathfinding,” in *Eighth Annual Symposium on Combinatorial Search*, 2015.

[46] W. Hönig, T. S. Kumar, L. Cohen, H. Ma, H. Xu, N. Ayanian, and S. Koenig, “Multi-agent path finding with kinematic constraints.” in *ICAPS*, 2016, pp. 477–485.

[47] L. Cohen, T. Uras, T. Kumar, H. Xu, N. Ayanian, and S. Koenig, “Improved bounded-suboptimal multi-agent path finding solvers,” in *International Joint Conference on Artificial Intelligence*, 2016.

[48] J. Yu and S. M. LaValle, “Optimal multi-robot path planning on graphs: Complete algorithms and effective heuristics,” *IEEE Transactions on Robotics*, vol. 32, no. 5, pp. 1163–1177, 2016.

[49] P. Hall, “On representatives of subsets,” *Journal of the London Mathematical Society*, vol. 1, no. 1, pp. 26–30, 1935.

[50] J. E. Hopcroft and R. M. Karp, “An  $n^{\frac{5}{2}}$  algorithm for maximum matching in bipartite graphs,” *SIAM J. Comput.*, vol. 2, pp. 225–231, 1973.

[51] M. Szegedy and J. Yu, “The  $n$ -Stacks Problem,” 2017, working manuscript.

[52] R. Cole, K. Ost, and S. Schirra, “Edge-coloring bipartite multigraphs in  $o(e \log d)$  time,” *Combinatorica*, vol. 21, no. 1, pp. 5–12, 2001.

[53] A. Goel, M. Kapralov, and S. Khanna, “Perfect matchings in  $o(n \log n)$  time in regular bipartite graphs,” *SIAM Journal on Computing*, vol. 42, no. 3, pp. 1392–1404, 2013.

[54] L. R. Ford and D. R. Fulkerson, “Maximal flow through a network,” *Canadian journal of Mathematics*, vol. 8, no. 3, pp. 399–404, 1956.

[55] S. D. Han, E. J. Rodriguez, and J. Yu, “SEAR: A Polynomial-Time Expected Constant-Factor Optimal Algorithmic Framework for Multi-Robot Path Planning,” *arXiv:1709.08215*, 2017.